The Clustering of Dark Matter in ΛCDM on Scales Both Large and Small

By

Chris Orban

Submitted to the Graduate School

in partial fufillment of the requirements

for the Ph.D. candidacy examination

Department of Physics

The Ohio State University

Columbus, OH

May 28, 2008

Contents

1 Introduction

This general cosmological picture of ΛCDM – of a universe composed primarily, of "cold" dark matter (CDM) particles and wherein a strange, repulsive energy, the cosmological constant (Λ), pervades all space – has been validated decisively in the last ten years by a flood of data from galaxy redshift surveys, direct measurements of the cosmological expansion history with Type Ia supernovae and precision mesaurements of the cosmic microwave background (CMB; Percival et al. 2007,Komatsu et al. 2008). With perturbation theory and numerical "N-body" simulations this model makes definite predictions for the clustering of the dark matter particles. In this review I describe the theory and observations of clustering of dark matter in the ΛCDM context, dividing the discussion into large (or cosmological, see e.g. Fig. 1) and small (i.e. galactic – see Fig. 2) scales.

Astronomers have known about dark matter for a long time. In a paper as far back as 1933, Fritz Zwicky used a back-of-the-envelope virial relation argument to show that the dynamically-inferred mass from measured peculiar velocities of galaxies in the Coma cluster disagree with a straightforward estimate of the mass from counting up cluster galaxies by a factor of 400 (Zwicky 1933). But it was not until the 1970s with work by Vera Rubin and others that it became clear, observationally, that this dark matter must be distributed differently than the stars (see Sofue & Rubin 2001 and references therein). This conclusion emerged from precise measurements of galaxy rotation curves, like the one shown for our Galaxy in the left panel of Fig. 2 (Klypin et al. 2002, see also Corbelli & Salucci 2000). Observations of the rates of microlensing events in the 1990s rejected the hypothesis of large populations of stellar remnants as the dark matter (Alcock et al. 1995), thus confirming the particle nature of the dark matter, and observations of galaxy clustering in the late 1980s and 1990s ruled out extremely light (dynamically "hot" – i.e. relativistic) particles as dark matter candidates (e.g. Weinberg & Gunn 1990; Geller & Huchra 1989).

Still viable is a massive dark matter particle in the $\sim$TeV$/c^2$ mass range with an extremely

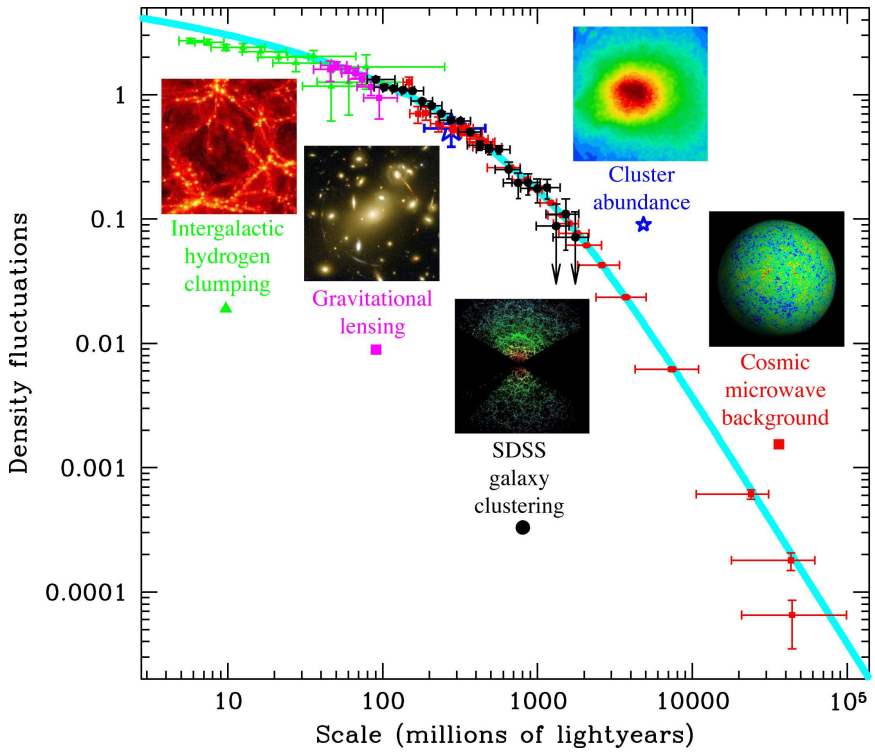

Figure 1: The Largest Scales: fluctuations around average matter density (y-axis) at different scales. Constraints on the fluctuations from various observations are also shown. (Figure from Max Tegmark's webpage, http://space.mit.edu/home/tegmark/ – data from Tegmark et al. 2004).

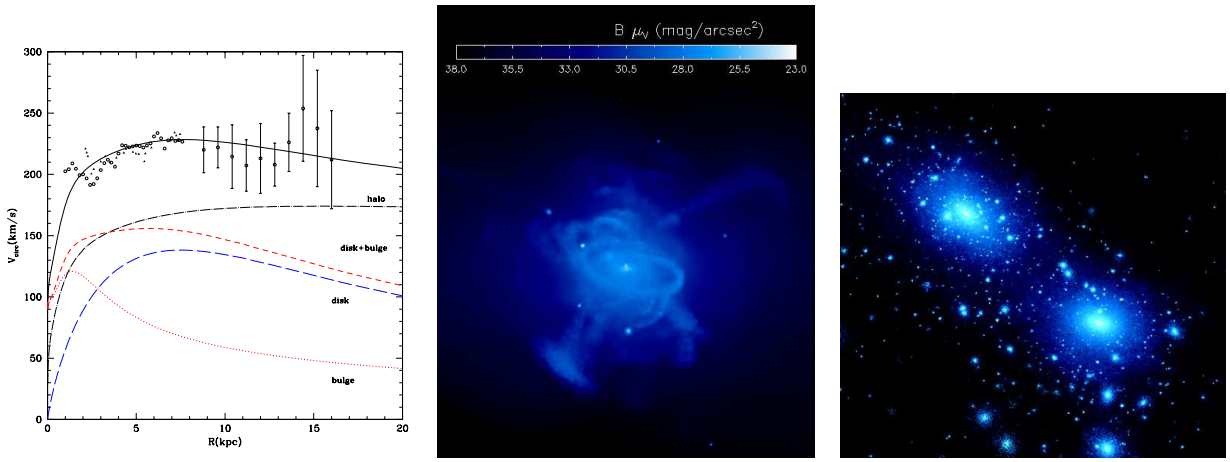

(a) Milky Way Rotation Curve (b) Near the Milky Way (c) The Local Group

Figure 2: The Small Scales: Left Panel – the Milky Way rotation curve (Klypin et al. 2002); Middle Panel – the outskirts of the Milky Way (Bullock & Johnston 2005); Right Panel – An N-body simulation of the Local Group (Klypin et al. 2001).

small matter cross section ($\lesssim 10^{-42}$ cm^2, e.g. Mack et al. 2007). Many popular beyond-the-standard-model theories of particle physics predict new particles to exist in this mass range, though, potentially, the mass can be much higher. For the purposes of the large-scale structure calculations that make up the bulk of this report, the particle must only be massive enough to be dynamically "cold" – in other words travelling non-relativistically, on average, in relation to a fixed observer at the present day – a condition met in the MeV/c^2 mass range and above. Also, in ΛCDM, the cross section of this particle must be small enough to be collisionless (well met by $\lesssim 10^{-42}$ cm^2).

In this review I describe the clustering of these particles, focusing on small scales – to be precise, smaller than about 10 million light years or ~ 3 Mpc – and large scales which, as Fig. 1 suggests, are larger than that mark to as large as 10^5 million light years or so. Physically, this boundary is motivated by making a distinction between the scales where galaxies (and associated dark matter) are caught up in the Hubble flow – i.e. where the observed radial velocity comes mostly from cosmological expansion – and scales where gravitational interactions predominantly govern the dynamics.

In § 2, I review what is known of the large scale clustering, in § 3 I discuss N-body simulations, an important numerical tool in understanding the dark matter distribution; in § 4 I discuss the small scale clustering of dark matter; I also review the usefulness of self-similar problems in § 5 – an important analytical tool – and give concluding remarks in § 6.

2 Large Scales

2.1 Dark Matter Density Evolution

To understand dark matter on large scales we must, as a first goal, take into account cosmological expansion and its effect on the overall dark matter density. The equations of general relativity admit a spatially-homogeneous solution where the linear size of the universe scales as a factor $a(t)$.

A useful characterization of this expansion is the Hubble rate:

$$H(t) \equiv \frac{da/dt}{a} \tag{1}$$

and the expansion rate depends on how much matter and energy there is (per unit volume) in the universe,

$$H^2(t) = \frac{8\pi G}{3}\rho = \frac{8\pi G}{3}[\rho_{\rm dm} + \rho_b + \rho_\Lambda + \rho_r] \approx \frac{8\pi G}{3}[\rho_{\rm m} + \rho_\Lambda], \tag{2}$$

where in the approximate expression I have made a late-universe assumption and neglected baryons ($\rho_{\rm dm} \approx \rho_m$ assumed here and throughout). Typically $\rho_{\rm m}$ and ρ_Λ are given as ratios over the critical density,

$$\rho_c = \frac{3H(t_o)^2}{8\pi G} = \frac{3H_o^2}{8\pi G} \tag{3}$$

$$\Omega \equiv \frac{\rho}{\rho_c} = \frac{\rho_{\rm m} + \rho_\Lambda}{\rho_c} = \Omega_{\rm m} + \Omega_\Lambda = 1 \tag{4}$$

where $\Omega = 1$ by assumption of flatness and consistency with general relativity (i.e. maintaining equality in Eq. 2). As the universe expands the average dark matter density becomes more dilute,

$$\rho_{\rm m} \propto a^{-3}. \tag{5}$$

Certain regions may become more dense or less dense over time, but, on average, the density field decreases like a gas of a finite number of particles in an expanding box.

2.2 Clustering

To understand the clustering of dark matter it is useful to define a density contrast,

$$\delta(\vec{x}) \equiv \frac{\rho_m(\vec{x}) - \overline{\rho}_m}{\overline{\rho}_m} \tag{6}$$

with $\overline{\rho}_m$ – the mean density of dark matter – falling as Eq. 5. From here we can define the two-point correlation function,

$$\xi(\vec{x}, \vec{x}') \equiv \langle \delta(\vec{x})\ \delta(\vec{x}') \rangle. \tag{7}$$

The brackets in this expression, and in subsequent expresions, are meant to represent the statistical (or "ensemble") average of the quantity enclosed. We can also work in Fourier space and consider the power spectrum of fluctuations,

$$\delta(\vec{k}) = \int d^3x \ \delta(\vec{x}) \ \exp\left(-i \ \vec{k} \cdot \vec{x}\right) \tag{8}$$

$$P(\vec{k}) \ (2\pi)^3 \ \delta_D(\vec{k} - \vec{k}') = \langle \ \delta(\vec{k}) \ \delta(\vec{k}') \rangle \tag{9}$$

where δ_D is the Dirac delta function and not to be confused with the density contrast, $\delta(\vec{x})$ or $\delta(\vec{k})$. Note that, by assumption of spatial homogeneity, $P(\vec{k}) = P(|\vec{k}|) \equiv P(k)$ and, similarly, $\xi(\vec{x}, \vec{x}') = \xi(|\vec{x} - \vec{x}'|) \equiv \xi(r)$. $P(k)$ has units of volume; we may be interested in a unitless quantity which describes the clustering,

$$\Delta^2(k) = \frac{k^3 \ P(k)}{2\pi^2} \tag{10}$$

The square root of this quantity (versus scale, rather than k) is what is plotted on the y-axis of Fig 1. And note that the power spectrum is simply related to the two-point correlation function,

$$\xi(r) = \int \frac{d^3k}{(2\pi)^3} \ P(k) \ \exp\left(i \ \vec{k} \cdot \vec{r}\right). \tag{11}$$

In this report I will discuss large scale structure strictly in terms of the power spectrum, rather than the correlation function. The two functions should, in principle, carry the same information (though in practice see Sirko 2005).

2.3 Galaxies

From an observational standpoint one of the best ways to learn about the clustering of dark matter is by observing the positions and redshifts of galaxies. As the CDM story goes, the dark matter, which is significantly more abundant than baryonic matter, collapses under gravity in the early universe, forming gravitationally-bound clumps called dark-matter halos. Gas (i.e. baryonic matter) will then fall into that potential well and, with high enough densities, forms stars and, with enough stars, forms the galaxies we see today. For the cosmologist this means that $P(k)$ must be inferred

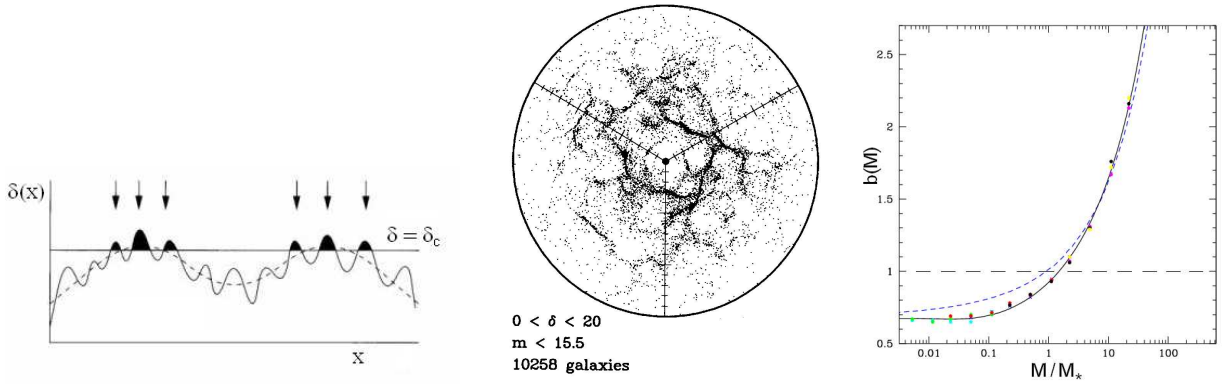

(a) 1-D density field (b) Biased Galaxy Field (c) Galaxy Bias, $b(M)$

Figure 3: Left Panel; a plot of $\delta(x)$ with a critical overdensity δ_c (illustration from Peacock 1999). Middle Panel: Biased Galaxy Density field from simulations by Weinberg & Gunn (1990). Right Panel: $b(M)$ vs M/M_* from Seljak & Warren (2004); $M_* \approx 10^{13} M_\odot$.

from a discrete distribution of points rather than a continuous density field. Furthermore, this distribution of points – the galaxies – may not be an accurate census of the underlying dark-matter density field, in other words it may be a "biased" tracer. There are two reasons for this: (1) unless the dark matter density field, $\delta(\vec{x})$, exceeds a certain value ($\delta_c = 1.686$, according to an idealized spherical collapse model – see Fig. 3(a), and Peacock 1999, pg. 488) the region around $\vec{x}$ will not collapse, thus preventing galaxies from being formed (technically, an antibias); and (2) the dark matter halos themselves are biased from the smooth dark matter distribution described by $P(k)$. The important point is that the galaxies end up more clustered or less clustered than the dark matter was to begin with, a fact conveyed by the preponderance of giant walls and voids seen in galaxy-redshift surveys, as illustrated in Fig. 3(b). In (Λ)CDM[1] this bias is quantified, to first order, by

$$\delta_h(M) = b(M)\ \delta_m(M) \tag{12}$$

[1] By this I mean in either ΛCDM or CDM, i.e. a universe with flat geometry, cold dark matter and with or without a cosmological constant.

where δ_h is the halo number density contrast and I have written these functions in terms of M; Eq. 12 holds for spherical regions which, at uniform cosmic density, contain mass M of dark matter. See Fig. 3(c) for specific values of $b(M)$.

2.4 The Power Spectrum

Enough is known about halo formation and galaxy bias from the theory side (e.g. Press & Schechter 1974; Sheth & Tormen 1999; Jenkins et al. 2001; Seljak & Warren 2004) that galaxy-redshift surveys can be uniquely interpreted to constrain $P(k)$. The theoretical power spectrum, in turn, depends on a variety of cosmological parameters. Of these $P(k)$ is particularly sensitive to σ_8 (to be discussed shortly) and Ω_m. The parameter σ_8 is the rms scatter of the dark matter density around the cosmic matter density in spheres of 8 h^{-1} Mpc in radius. More formally,

$$\sigma^2(R) = \int \frac{dk}{k} \frac{k^3 P(k)}{2\pi^2} |W(kR)|^2 \tag{13}$$

where $W(kR)$ is the window function for a sphere of radius R; $\sigma_8 \equiv \sigma(R = 8h^{-1}$ Mpc). The effect of changing σ_8 is to raise (by increasing σ_8) or lower (by decreasing σ_8) the overall normalization of $P(k)$ as in Fig. 4.

Changing Ω_m changes $P(k)$ in that Ω_m, along with Ω_r and H_o, fixes the epoch of matter-radiation equality, namely when $\rho_r = \rho_m$ in the early universe. As I will discuss in the next section, perturbations grow very differently in the time period before this point – the radiation-dominated era – than in the period after this point – the matter-dominated era. So the precise time when one era begins and the other ends will have an important effect on the clustering we observe today. The bottom line is that raising Ω_m shifts the peak of $P(k)$ towards the right, and lowering Ω_m shifts it to the left (see Fig. 4).

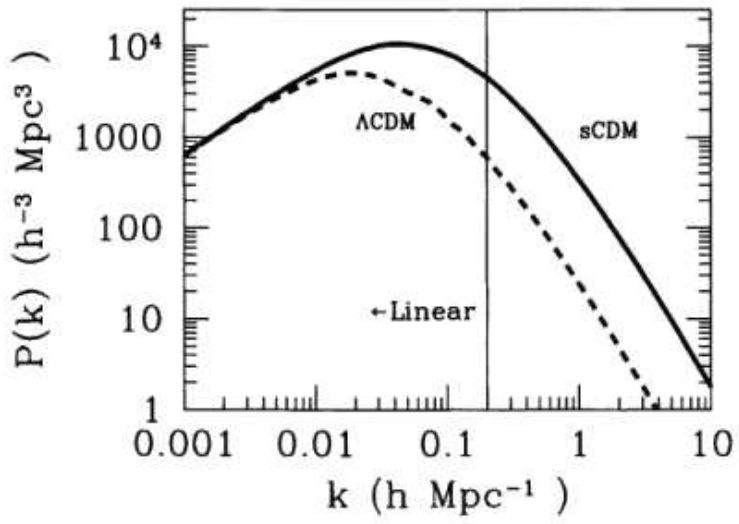

Figure 4: The power spectrum for ΛCDM ($\Omega_m = 1 - \Omega_\Lambda \approx 0.3$) compared to the power spectrum for sCDM ($\Omega_m = 1$, $\Omega_\Lambda = 0$). The non-linear wave number, $k_{\rm nl}$, is indicated with a vertical line (see § 2.6). Figure from Dodelson (2003).

2.5 How's and Why's

In the discussion so far I have sidestepped explaining the growth of perturbations, instead focusing on the dark matter clustering today and the complications of inferring that from the observed galaxy distribution. The goal of this section is to explain how perturbations grow in CDM, to explain why $P(k)$ has the general shape that it does, and in the process substantiate the claim made in the previous section about the effect of changing Ω_m on $P(k)$.

As I mentioned in the last section, perturbations grow at very different rates during the radiation-dominated epoch than in the matter-dominated epoch. In both eras we can write down the Euler equations, as with any fluid, adding in the expansion of the universe and end up with a second-order differential equation for δ (see Peacock 1999, §15.2). During the matter-dominated era this gives,

$$\frac{\partial^2\delta}{\partial t^2} + 2\,\frac{da/dt}{a}\,\frac{\partial\delta}{\partial t} = 4\pi G\rho_m\,\delta - \frac{k^2c_s^2}{a^2}\,\delta. \tag{14}$$

where c_s is the sound speed of our cosmological fluid. And during the radiation-dominated era a

similar analysis gives,

$$\frac{\partial^2\delta}{\partial t^2} + 2\ \frac{da/dt}{a}\ \frac{\partial\delta}{\partial t} = \frac{32\pi G\rho_r}{3}\ \delta - \frac{k^2c^2}{3a^2}\ \delta. \tag{15}$$

The primary difference between the two eras is that the sound speed during the radiation-dominated era is very fast, $c_{s,\mathrm{rad}} = c/\sqrt{3}$, whereas during the matter-dominated era, c_s, which is at this point typical of baryonic gas sound speeds, is much smaller. As a result, during the radiation-dominated era, even fairly small values of k allow the k^2 term to overwhelm the other terms, i.e.,

$$\frac{\partial^2\delta}{\partial t^2} = -\frac{k^2c^2}{3a^2}\ \delta \tag{16}$$

which is solved, simply enough, by $\delta = Ae^{i\omega t}$ where $\omega = kc/\sqrt{3}a$. The important thing is that A is a constant which does not increase in time. By contrast, at very small k, we have

$$\frac{\partial^2\delta}{\partial t^2} + 2\ \frac{da/dt}{a}\ \frac{\partial\delta}{\partial t} = \frac{32\pi G\rho}{3}\ \delta \tag{17}$$

which is solved by $\delta \propto t^{\pm 1}$. The t^{-1} solution will decay away but the $\delta \propto t$ solution will grow in time. So, in the end, we expect perturbations above a certain "fairly small" k to be essentially stagnant, and perturbations below a certain, smaller, k-value to grow. In (Λ)CDM it is believed that the power spectrum starts from $P(k) \sim k$ over all k at the very beginning of the radiation-dominated era, so the overall shape of the power spectrum at the end of that era is, in effect, what survives of that input signal after being put through a low-pass filter and amplifier. The matter-dominated era simply amplifies the perturbations left behind by the radiation-dominated era without changing the overall shape of $P(k)$ – i.e., notice that $\delta \propto t^{2/3}$ solves Eq. 14 for all $k \ll \sqrt{4\pi G\rho_m}/c_s a$. The power spectrum we observe today is thus a snapshot, in a sense, of the power spectrum at the end of the radiation-dominated era.

2.6 Disclaimer!

Though well beyond the scope of the present review it is worth mentioning that the previous section relies on a pseudo-Newtonian approximation to General Relativity and that there is a thriving

industry around developing more theoretically precise and physically-accurate mathematical descriptions of $P(k)$. In the literature this is the quest for the "transfer function", which is a function meant to be multiplied by the original power spectrum from inflation ($P(k) \sim k$, as mentioned earlier) to give something that, when amplified by a constant factor from gravity, gives the $P(k)$ we observe today. Dodelson (2003) (§7) presents a detailed description of this function which can include the subtle effect of baryons on the power spectrum or the effect of neutrinos (also subtle). In focusing on dark matter, and on the most important influences on $P(k)$ I have left these two effects out of the present discussion.

Finally, it should also be mentioned that the differential equations in the previous section are only true in the $|\delta| \ll 1$ limit; those equations were derived by a linearizing approximation to the Euler equations and so are not always true. However for most of the k-values we are interested in those equations are close to correct and the value of k where our analytic approximations fail is simply $\Delta^2(k_{\rm fail}) = k_{\rm fail}^3 P(k_{\rm fail})/2\pi^2 \equiv 1$. More optimistically, this value of k, referred to as $k_{\rm nl}$ indicated in Fig. 1, is where we have little choice but to investigate the non-linear regime with N-body simulations. I will return to this theme in § 5.

2.7 Measurements of the Power Spectrum

Given the wide variety of observations and detailed statistical methods for constraining the power spectrum, my review of these measurements will be unavoidably brief and qualitative. I have already explained in some detail the relationship between the dark matter clustering and the galaxy clustering in § 2.3. Figure 1 shows, in black points, the constraints on the dark matter clustering inferred from the galaxy clustering in the Sloan Digital Sky Survey (SDSS) after compensating for galaxy bias. The positions and redshifts of almost a million galaxies make those error bars as tight as they are.

Figure 1 also shows the results from other measurements, such as the abundance of galaxy clusters – the most massive gravitationally-bound structures in the universe. The general idea is

that N-body simulations allow us to make very precise predictions of the number and masses of very-massive dark matter halos given a set of cosmological parameters. This theory predicts the number of galaxy clusters that should be detectable in the night sky, so by taking the observed number of clusters one can compare to these predictions and say something meaningful about Ω_m and σ_8. (In the next chapter I will explain more of what goes into the calculation of the numbers and masses of dark matter halos.) As a final remark on these measurements, though there is some information about $P(k)$ in the spatial clustering of the galaxy clusters (Lima & Hu 2004), but for the most part, since clusters are relatively rare objects in the sky, these observations speak more to the overall matter density or the overall level of clustering (through determining σ_8) than to the clustering on a variety of length scales.

At smaller scales than galaxy-redshift surveys, weak gravitational lensing provides unique constraints on $P(k)$ by measuring the deflection of star light from the underlying dark matter distribution. As such, weak lensing has the advantage of being free of the usual worries about inferring the dark matter distribution from the galaxy distribution. The trick is to observe the shapes of distant galaxies, by looking closely at the shapes of distant galaxies. Since these background galaxies are ellipsoidal, to good approximation, deviations from this shape can reveal the influence of the intervening dark matter. As Fig. 1 reports, there are already some very interesting constraints on $P(k)$ from these measurements. For more recent constraints see, e.g., Massey et al. (2007).

Another important constraint on $P(k)$ that deserves mention is from the Lyman-α "forest". Here the observation is of a distant quasar with bright Lyman-α emission (a spectral line of Hydrogen). The signal in the higher-wavelength wings of this emission is very sensitive to the amount of intergalactic hydrogen gas, at a certain redshift, between the observer and the source. The effect of this gas shows up as many sharp absorbtion features in the spectrum of the quasar – hence the name "forest". The important point here is that this spectrum is sensitive to the gas and associated dark matter which has not collapsed under gravity. This allows the spectra to be interpreted to higher k without worrying about bias factors and other complications as in §2.3. With the galaxy distribution

the very high-k information is difficult or impossible to extract because typical halo densities are well into the non-linear regime where the analysis becomes much harder. The discussion in previous sections of this chapter is a outline of how the galaxy distribution is used to probe dark matter fluctuations on scales much larger than the spacing of the galaxies themselves – i.e. of much lower k.

Last, but by no means the least, the CMB can constrain $P(k)$ on the very largest scales. Since the CMB reveals the amplitude of perturbations from when the universe was much smaller it tells us about scales which are now much larger than we can easily observe. In particular it is our primary source of information for the modes which were larger than the horizon scale during the radiation-dominated epoch, as discussed in § 2.5. For the latest measurements see Komatsu et al. (2008).

3 N-body Simulations

3.1 Overview

N-body simulations, in the broadest sense, aim to replicate, on a computer, the interactions of many particles. These particles, to name a few examples, can be atoms, stars, ions, fluid elements or dark matter particles, and the interactions can be electromagnetic, hydrodynamical or, in the case which concerns us here, gravitational.

In astrophysics, N-body simulations go back a long way. Erik Holmberg, in 1941, used the flux from 37 lightbulbs and photocells to simulate the gravitational inverse square law forces between two interacting spiral galaxies. The advent of the digital computer in the 1960s opened the door to using N-body simulations to attack a variety of astrophysical problems and, in 1974, William Press and Paul Schechter used an N-body simulation with 1000 particles to simulate, for the first time, the formation of structure in an expanding universe (see the introduction of Bertschinger 1998 for an historical review). Since then, through Moore's law, the development of parallel computing and

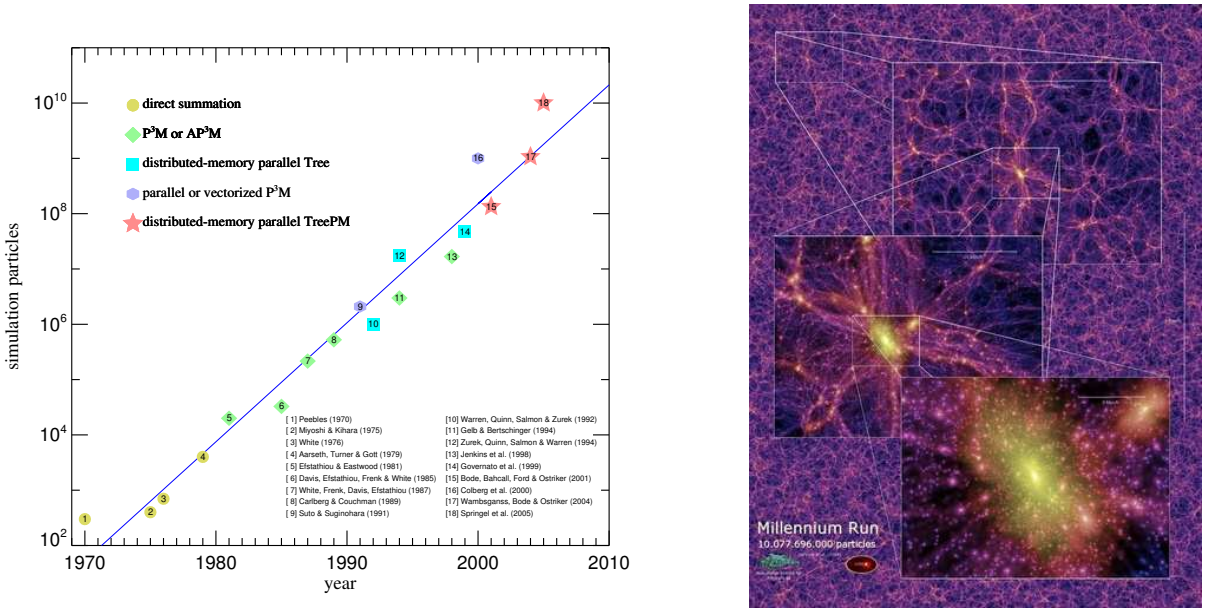

Figure 5: Left: A plot of N, the number of simulated particles, versus year for various cosmological simulations (from Springel et al. 2005). Right: A visualization of the Millenium Simulation on different scales, one of the largest cosmological N-body simulations to date (Springel et al. 2005).

cleverly-designed algorithms the cutting-edge N has grown fantastically larger (See Fig. 5(a)). The current world record for a cosmological simulation is the Horizon Simulation[1] with $N \approx 7 \times 10^{10}$, i.e. 70 billion particles. The runner up is the Millenium Simulation (Fig. 5(b)) with $N \approx 10^{10}$.

Despite these technologial advances there are still important limitations inherent in these simulations. The typical mass of an N-body particle is still, inescapably, much larger than the expected mass of the dark matter particle ($m_\chi \sim 100$ GeV). Consider a box of 1 Gpc^3 in volume with a cosmic dark matter density and $N = 4096^3 \approx 7 \times 10^{10}$ particles.

$$m_N = \frac{\bar{\rho}_m V}{N} = \frac{\Omega_m \rho_c \ 1 \ \mathrm{Gpc}^3}{7 \times 10^{10}} \approx \frac{10^{11} M_\odot \mathrm{Mpc}^{-3} \mathrm{Gpc}^3}{10^{11}} = 10^6 \ M_\odot \tag{18}$$

which is clearly much larger than reasonable expectations for elementary particles. However, the total dark matter halo mass of galaxies is thought to be roughly $\sim 10^{12} \ M_\odot$, so for the purposes of large-scale strucutre and other dynamical problems this limitation should not invalidate our results.

[1] http://www.projet-horizon.fr/article323.html

Mindful of the need to accurately predict $P(k)$, N-body simulations are also limited on small and large scales because of the finite box size. With a Gpc^3 box, for example, it will not be possible to speak meaningfully about modes $k \lesssim 2\pi/\mathrm{Gpc}$. Nor will it be possible to know $P(k)$ for $k \gtrsim \pi/\Delta x = k_{\rm Ny}$, where Δx is the grid spacing.

3.2 Halo Mass Function

As mentioned in § 2 one of the primary uses of N-body codes is to go beyond idealized analytic estimates for the gravitational collapse of dark matter halos. I discussed the bias in § 2.3; suffice it to say that N-body simulations more precisely determine $b(M)$ (see, e.g., Seljak & Warren 2004; Zentner 2007). In this section I will discuss the halo mass function, and an analytic derivation of its form.

The halo mass function is very often discussed in terms of a halo number density per unit mass, dn/dM. To get this I will assume, following Press-Schechter theory, that δ is randomly distributed as a gaussian with mean zero and an rms of $\sigma^2(R)$ as in Eq. 13. The fraction of the cosmological volume that has collapsed is then,

$$f_{\rm coll} = \frac{2}{\sqrt{2\pi}\sigma(R)} \int_{\delta_c}^{\infty} \exp\left(-\frac{\delta^2}{2\ \sigma^2(R)}\right)\ d\delta \tag{19}$$

where R is the smoothing radius. (For those curious about the factor of 2 see Zentner 2007, pg. 10). In § 2.3 I mentioned that by assuming a cosmic density one can go between M and R; $M(R) = \bar{\rho}_m\ 4\pi R^3/3$. Invoking that here the number density of collapsed objects with mass between M and $M + dM$ is

$$dn(M)\ = -\frac{\bar{\rho}_m}{M}\ \frac{df_{\rm coll}}{dM}\ dM \tag{20}$$

where, logically, ρ_m/M is the maximum number of objects of mass M which can exist in a certain volume at cosmic density ρ_m; the remaining terms are the fraction of these objects which have collapsed. (Note $df_{\rm coll}/dM < 0$, hence the (-) sign.) It can be shown,

$$\frac{dn}{dM} = \sqrt{\frac{2}{\pi}}\frac{\bar{\rho}_m}{M^2}\frac{\delta_c}{\sigma}\exp\left(-\frac{\delta_c^2}{2\sigma^2}\right)\left[-\frac{M}{\sigma}\frac{d\sigma}{dM}\right] = \frac{\bar{\rho}_m}{M^2}\nu f(\nu)\left[-\frac{M}{\sigma}\frac{d\sigma}{dM}\right] \tag{21}$$

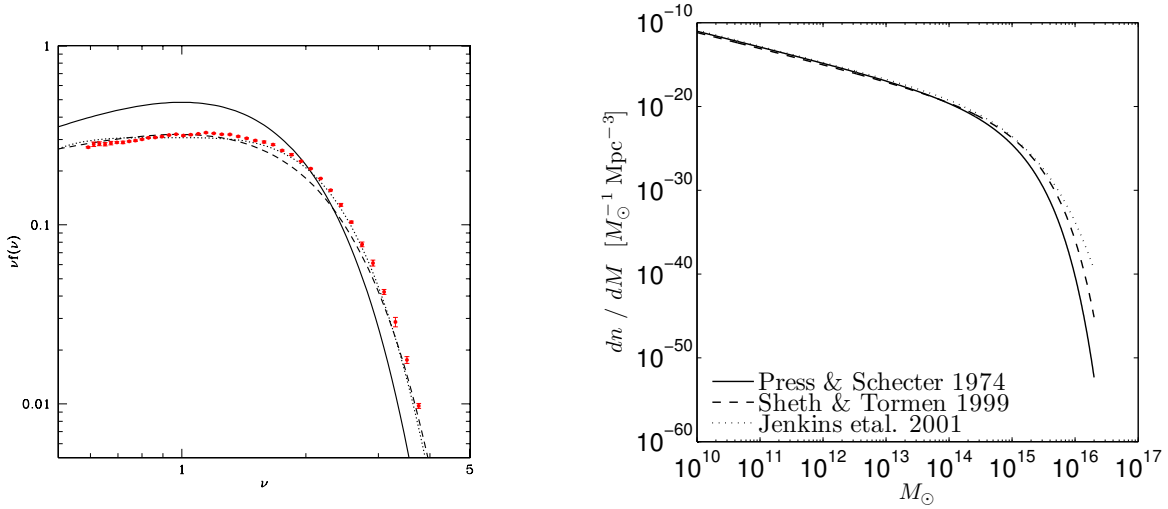

Figure 6: Left: a plot of the collapsed mass fraction, $\nu f(\nu)$, for the analytic models of Press & Schechter 1974 (solid line), Sheth & Tormen 1999 (dashed), and the numerical fit from Jenkins et al. 2001 (dotted line), (Figure taken from Zentner 2007). Right – The halo mass function with those three different prescriptions for the collapsed mass fractions (same line styles) for parameters: $\Omega_m = 0.3$, $\Omega_\Lambda = 0.7$, $\sigma_8 = 0.8$, $H_o = 70$ km s^{-1}.

It turns out $\nu f(\nu)$ is a function (which obviously describes halo collapse) that is almost completely independent of cosmological parameters (e.g. Fig. 7 of Jenkins et al. 2001). N-body simulations can determine this function better than analytic treatments can. Fig. 6(a) from Zentner (2007), illustrates this by comparing two analytic formulae (Press & Schechter 1974 – the black line, and Sheth & Tormen 1999 – the dashed line) to a fit to N-body simulation (Jenkins et al. 2001 – the dotted line). Fig. 6(b) shows that these different functions make different predictions for the halo mass function.

3.3 Closer to Home

In § 4 I will discuss what is known of the clustering of dark matter on small scales, cosmologically speaking. Here I comment only to say that there are various tricks and other methods used to obtain higher mass and spatial resolution, such as resimulating a small chunk of a larger simulation with a large number of particles (e.g. Klypin et al. 1999; Diemand et al. 2007) or approximating

the gravitational effect of the Milky Way with an analytic potential and devoting the bulk of the computational power to simulating dwarf galaxy accretion events (e.g. Bullock & Johnston 2005). In any case, the sumulations which describe the clustering of dark matter on small scales all take into account this larger cosmological backdrop in some way. And again, from the theory side, N-body simulations allow us to investigate regimes where analytic answers are hard, if not impossible, to come by. A good example is the "universal" halo density profile (Navarro et al. 1997),

$$\rho_{\rm NFW}(r) = \frac{\rho_o}{\frac{r}{r_s}(1+\frac{r}{r_s})^2} \tag{22}$$

which is an empirical fit to N-body simulations. It is not, in general, possible to find an analytic prediction for this function, though many would be interested to know the small r behavior of such an expression since it has important implications for the expected dark matter annihilation signal.

4 Small Scale Clustering

The most compelling evidence for dark matter is the rotation curves for spiral galaxies. The rotation curve is a plot of the speed at which stars or gas move around the center of a galaxy. Fig. 2(a) shows the rotation curve for our own Galaxy, which is very typical of other spiral galaxies. The feature to notice is the trend for $V(r)$ to flatten out at large radii. Dynamically, from Newtonian Gravity, we expect $V(r) = \sqrt{2GM(<r)/r}$ where $M(<r)$ is the mass enclosed in some radius from the galactic center, so the most straightforward explanation of this is that $M(<r) \sim r$. This, in turn can be naturally accounted by integrating $\rho_{\rm NFW}$ from Eq. 22.

$$M(<r) = 4\pi \int_0^r \rho_{\rm NFW}(r') r'^2 dr' = 4\pi\rho_o \int_0^r \frac{r'^2}{(\frac{r'}{r_s})(1+\frac{r'}{r_s})^2} dr' \tag{23}$$

if $r \ll r_s$ we can approximate this by

$$M(<r) \;\approx\; 4\pi\rho_0 r_s \int_0^r r' dr' = 2\pi\rho_0 r_s r^2 \propto r^2. \tag{24}$$

If, instead, $r \gg r_s$ then, to order of magnitude,

$$M(<r) \approx 4\pi\rho_0 r_s \int_0^{r_s} r' dr' + 4\pi\rho_0 r_s^3 \int_{r_s}^{r} \frac{dr'}{r'} = 2\pi\rho_0 r_s^3 + 4\pi\rho_0 r_s^3 \ln\left(\frac{r}{r_s}\right) \propto \ln\left(\frac{r}{r_s}\right) \tag{25}$$

So, the result is something that behaves like $M(<r) \propto r^2$ for small r and $M(<r) \propto \ln(r/r_s)$ for large r; between these extremes is exactly what we need to explain the observed $M(<r) \sim r$. This sort of behavior has been confirmed for hundreds of spiral galaxies now with a variety of observations.

4.1 Dwarf Galaxies

The very first quantitative suspicions that there might be significant amounts of dark matter in the universe came from virial relation arguments applied to the Coma cluster by Zwicky (1933). Here I will use that same argument to show that dwarf galaxies in the Local Group are dark-matter dominated systems by showing that they have high mass-to-light ratios.

The virial relation for relaxied (a.k.a. "virialized") systems is

$$2KE_{\rm total} = -PE_{\rm total} \tag{26}$$

and in the case of dwarf galaxies it is the total kinetic and potential energies of the stars, rather than the galaxies as in the Coma cluster, which will give us our mass estimate. Very roughly, then,

$$2KE_{\rm total} \approx MV^2 \sim \frac{GM^2}{R} \approx PE_{\rm total}. \tag{27}$$

For dwarf galaxies, as a typical number, $R \sim 500$ pc as the size of the dwarf and, from the observed radial velocities of the stars, $V \sim 30$ km s^{-1}. So,

$$M \sim \frac{RV^2}{G} \sim 10^7 M_\odot. \tag{28}$$

Luminosities for Local Group dwarfs are typically $L_V \ll 10^7 L_\odot$, especially for the R and V assumed here. It is clear, then, that

$$\frac{M}{L_V} \gg 1. \tag{29}$$

Dwarf galaxies are, in fact, the most dark-matter dominated galaxies which makes them ideal targets for observing the dark matter annihilation signal over astrophysical backgrounds (see Aharonian et al. 2008 for γ-ray observations of the Sagittarius dwarf; see Strigari et al. 2008 for predicted fluxes). But so far no flux excess has been observed – only upper limits have been placed.

4.2 The Substructure Problem

Bearing in mind the connection between dwarf galaxies and dark matter, it was a very suprising thing when N-body simulations of the Local Group indicated that there should be many more small dark matter halos (called subhalos or substructure) near the Milky Way than a simple count of the number of dwarf galaxies (a few dozen) would indicate (Kauffmann et al., 1993; Klypin et al., 1999; Moore et al., 1999). This discrepancy is shown visually in Fig. 7. and quantitatively in Fig. 8 from Strigari et al. (2007).

The night sky has been searched very thoroughly for dwarf galaxies (Koposov et al. 2007) and though there may be more to discover the discrepancy is so sever that it is very unlikely that the disagreement can be resolved this way. One possibility – and certainly the most conservative option – is that dwarf galaxy formation is very complicated and easily supressed. In other words the simulations are right about the nearby clustering of dark matter but that for a variety of reasons (e.g. reionization, gravitational interactions) the dark matter (sub)halos remain dark. Another possibility is that ΛCDM is wrong and that the nearby clustering of the dark matter is very different from ΛCDM expectations. This may be because the dark matter particle mass is much lower than previously thought (Zentner & Bullock 2003) or that dark matter is self-interacting (Spergel & Steinhardt 2000) or that the inital $P(k) \sim k$ power spectrum mentioned in §2 has a sharp cutoff at some high value of k (Kamionkowski & Liddle 2000). The jury is still out on which of these options, if any, is the culprit – though see §4.4. Generally, the supression of dwarf galaxy formation in cold dark matter halos is thought to be the most natural resolution to this discrepancy, often referred to in the literature as the "substructure" or "missing satellite" problem.

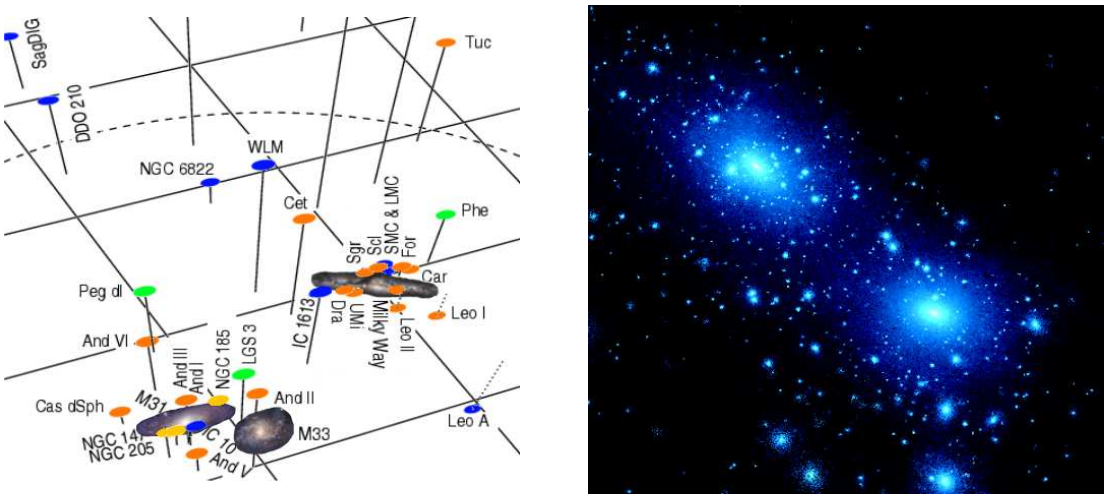

Nearby Dwarf Galaxies in the Local Group

N-body Simulations

Figure 7: Left panel – Images of the three spiral galaxies in the Local Group are shown; the colored ovals are all dwarf galaxies. (Figure adapted with permission from E. Grebel.) Right panel – output from an N-body simulation of the Local Group. System approximately corresponds to the Milky Way (MW) and Andromeda (M31). (Used with permission from A. Kravtsov.)

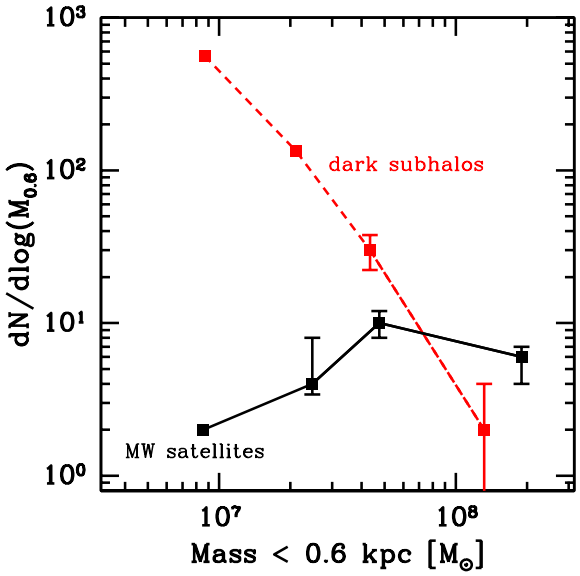

Figure 8: The missing satellites problem as defined by Strigari et al. (2007). Compared is the enclosed mass within $r = 0.6$ kpc for cold dark matter (sub)halos and observed dwarf galaxies in the Local Group. Figure used without any permission whatsoever from L. Strigari.

4.3 Tidal Streams

In recent years there has been much excitement around the discovery of faint streams of stars around Andromeda (Ibata et al. 2001) and the Milky Way (Ibata et al. 2001) which seem to be associated with the disruption of dwarf galaxies. In the ΛCDM paradigm the existence of these systems is an important confirmation of hierarchical structure formation – the theory that large galaxies grow from the bottom up by accreting smaller galaxies. In one particular study "How Lumpy is the Milky Way's Dark Matter Halo?" (Johnston et al. 2002) N-body simulations with and without substructure were used to argue that the stars in the Sagittarius stream (Ibata et al. 2001), which extends over a large part of the Milky Way, seem to be more scattered on the sky and less of a coherent structure than a smooth halo model would predict. Simulations like these have grown considerably more sophisticated since then (see, e.g., Fig. 2(b)) in anticipation of Sloan III (Weinberg et al. 2007) which will map the tidal streams in the Milky Way with even greater detail.

4.4 Strong Gravitational Lensing

Acknowledging the existence of dark matter in large quantities but treating with skepticism the evidence presented so far for substructure, strong gravitational lensing may be the only way to directly[1] detect whether galaxies like the Milky Way are surrounded by a host of dark matter subhalos. I have already mentioned in the introduction that gravitational microlensing was integral to rejecting MACHOs as the source of the dark matter – I will not elaborate on that here. Instead I will summarize the state-of-the-art in strong gravitational lensing which actually claims to have detected substructure (Dalal & Kochanek 2002).

A system can be said to be strongly lensed when the observer-lens-source geometry is such that the observer sees arcs and/or multiple images of the source as in the four-image quasar lens system shown in Fig. 9. Four-image systems are very useful, astrophysically, since the positions

[1] Here, for salesmanship, I assume the astronomer's understanding of direct detection, rather than the physicist's.

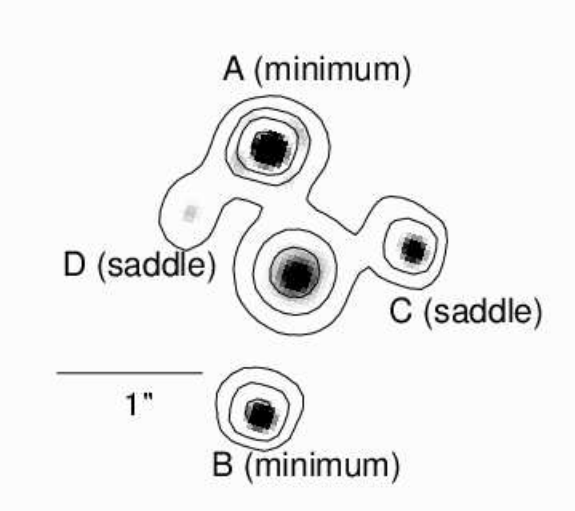

Figure 9: The most spectacular example of a four-image quasar lens system with an anomalous flux ratio (Inada et al. 2003). Image D, assuming no substructure, should be as bright as Image A. See text for discussion.

of the images, which can be measured very well, and the fluxes provide strong constraints on the gravitational potential of the object doing the lensing. By using this information to solve for the size and ellipticity of the lens, assuming a smooth-potential model, astronomers hoped to determine H_o completely independently of any other observation by measuring the differences of the path lengths travelled by the light with the time delay between images. But, fortunately or unfortunately, these smooth-potential models as well as higher-order multipole models failed to match the observed fluxes in the known lenses (Evans & Witt 2003; Kochanek & Dalal 2004; Congdon & Keeton 2005). There is some debate around whether these "anomalous" flux ratios are real, in the sense of being caused by the substructure, or whether they were caused by contamination or opacity from the lens galaxy or from the effect of stellar microlensing, which can temporarily change the flux ratios on the timescales of decades. Kochanek & Dalal (2004) argue that the observed four-image quasars should be relatively unaffected by these concerns and that the flux ratios can be legitimately caused the substructure.

In any case, the discussion of flux contamination aside, of the six known four-image quasar lens systems known at the time of Dalal & Kochanek (2002), five of them had significant flux anomalies.

Using this fact Dalal & Kochanek ran Monte Carlo simulations of four-image lens systems with different levels of substructure or no substructure at all to show, in a statistical way, that the flux anomalies can be explained by adding substructure whereas the no-substructure model is strongly disfavored.

In the future these kinds of investigations will benefit from the discovery of new multiple-lens systems with next-generation surveys. There is some hope, even, to further constrain the substructure with very precisely-measured time delays (Keeton & Moustakas 2008). However the leap must be order of magnitude in both temporal precision and the number of known lenses to do significantly better than what is possible now. The literature often mentions the need for "revolutionary data sets" to take this kind of analysis to the next level.

5 Self Similarity

5.1 Motivation

In §2.6 I mentioned that for $k > k_{\rm nl}$ analytic and ordinary differential equation solvers can no longer accurately model the real $P(k)$. As long as $k < k_{\rm Ny}$, N-body simulations should have no trouble picking up where these approximations left off. However it raises an important question: how do we know that the N-body simulations are successfully modeling this regime? With this worry in mind Efstathiou et al. 1988 set out to test their N-body code with scale-free initial conditions[1]; so if the initial conditions do not include a characteristic scale then there should be a self-similar (a.k.a. scaleable) solution to the problem. This solution, unlike the equations in §2.5, will extend into the non-linear regime and provide a useful test of the N-body code.

[1] In my opinion the phrase "scale-free" initial conditions is misleading. Though in $P(k) = A\,k^n$ no k in particular is singled out, the constant, A, does set a fundamental scale – the clustering amplitude of the initial conditions. Nowadays we determine A by σ_8, an input cosmological parameter, so the argument here is somewhat semantic.

5.2 Quantitatively

Ideally, without any approximations, N-body simulations seek to determine the phase space evolution of the dark matter, $f(\vec{x},\vec{p},t)$, according to the following partial differential equation (the Vlasov equation)

$$\frac{\partial f(\vec{x},\vec{p},t)}{\partial t} + \frac{p^i}{ma^2}\frac{\partial f}{\partial x^i} - m\frac{\partial \phi}{\partial x^i}\frac{\partial f}{\partial p^i} = 0 \tag{30}$$

and an integro-differential equation (the Poisson equation),

$$\nabla^2\phi = 4\pi G m a^{-1}\int f\ d^3p \tag{31}$$

where i, the coordinate index, is summed over and $a \propto t^{2/3}$, as is usual for a matter-dominated universe. It turns out (as asserted by Peebles 1980, §73) that the above equations admit a "scalable" solution,

$$f(\vec{x},\vec{p},t) = t^{-3\beta}\hat{f}(\vec{x}/t^\alpha,\vec{p}/t^\beta) \tag{32}$$

if, and only if,

$$\beta = \alpha + 1/3. \tag{33}$$

Notice, in Eq. 32, instead of a function of three quantities, $\vec{x},\vec{p}$ and t, we have a function of only two quantities. This function is not generally derivable from first principles, but it nevertheless is a useful simplification of the problem without making any approximations to Eqs. 30 & 31. How does this connect to scale-free initial conditions, $P(k) = Ak^n$? Well, the derived quantities that we will be interested in – i.e. $\xi(r)$ and $P(k)$ – involve integrating out the momentum variable so, effectively, we can consider just the spatial scaling of the problem, $x \rightarrow x/t^\alpha$, and convince ourselves that $\xi(x) \rightarrow \hat{\xi}(x/t^\alpha)$. Now if we take the inverse fourier transform of Eq. 11,

$$P(k) = \frac{1}{2\pi^2}\int \xi(x)e^{i\vec{k}\cdot\vec{x}}d^3x \tag{34}$$

with scale-free initial conditions (with $\delta \propto t^{2/3}$ time dependence) and our scalable solution this becomes,

$$At^{4/3}k^n = \frac{1}{2\pi^2}\int \hat{\xi}(x/t^\alpha)e^{i\vec{k}\cdot\vec{x}}d^3x \tag{35}$$

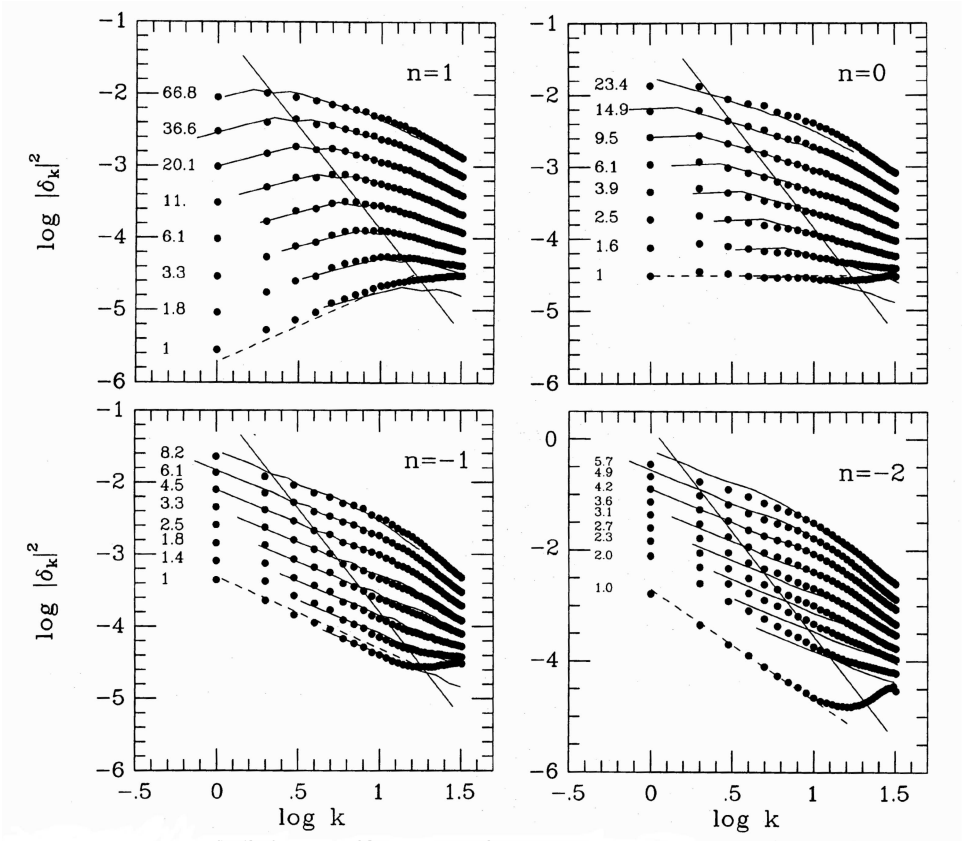

Figure 10: Power spectra from N-body simulations with different initial conditions, $P(k) = A\,k^n$ (dashed line). Simulation measurements (black dots) at different times (higher lines are later timesteps than lower lines) are compared to the self-similar solution (black line), which are matched to the third to the last time step and scaled to other times. The non-linear scale, which becomes larger over time, is shown with a steep, diagonal black line. All the simulation results to the right of this line are probing a regime inaccessible to perturbation theory.

and by substituting $x' = x/t^\alpha$ this becomes,

$$At^{4/3}k^n = \frac{1}{2\pi^2}t^{3\alpha}\int \hat{\xi}(x')e^{it^\alpha \vec{k}\cdot\vec{x}}d^3x. \tag{36}$$

Finally, with yet another change of variables $s = t^\alpha k$, we can throw all the k-dependence on one side and set it equal to a constant and show,

$$\alpha = \frac{4}{9+3n}. \tag{37}$$

The virtue of this solution is that it remains true even in the deeply non-linear regime. And, the results, as shown in Fig. 10 from Efstathiou et al. (1988), from simulating exactly this kind of solution convinced the field that the N-body simulations were getting things right in the non-linear

regime to begin with.

5.3 Self-Similarity in ΛCDM

How applicable is this result for the ΛCDM universe we seem to be living in? The bad news is that the dark energy does introduce a fundamental scale into the problem. Though, typically, this scale is thought of as some fantastically small vacuum energy density it is also correct (and more intuitive in my opinion) to say that dark energy is a force that accelerates the universe's expansion only when the universe has reached a certain size. This means that, in terms of direct applicability, the self-similar solution will only be relevant for the matter-dominated ($\Omega_m \approx 1$) era, which ended a few billion years ago. The clustering of high-redshift galaxies, for example, could still, on certain scales, be modeled by the results here. For the most part, though, the enduring value of self-similar initial conditions remains in its usefulness as numerical test problem in large-scale structure. There are other tests, to be sure, but they may be a step further removed from what we are actually using the codes to do.

As long as no new fundamental scale is introduced, it is possible to test N-body + hydrodynamics codes for galaxy formation and Lyman-α forest measurements with this kind of procedure (Owen et al. 1998a,b; Abadi et al. 2000; Uchida & Yoshida 2004). In the arena of running massive cosmological simulations these sorts of tests have been ignored in recent years; groups have opted to use the standard ΛCDM initial conditions and assumed the best in analyzing the output and measuring $P(k)$. An interesting potential project would be, for example, to investigate the subhalo population in large N-body simulations with scale-free initial conditions since getting the large-k power spectrum right – the smallest scales – is a related problem to determining the subhalo mass function. Another idea would be to carry out an ensemble of simulations, as prescribed by Sirko (2005), with an analytic scale-free solution in hand to quantify the accuracy of $P(k)$ at *low* k. This sort of project would have interesting rammifications since the ethos of the cosmological simulation community is to perform one very large simulation, rather than performing many smaller

simulations with different random seeds and subtly different values of Ω_m and pasting those results together to learn about the clustering on the very largest scales. It is not clear, at the moment, which method is the more robust and efficient.

6 Summary and Conclusion

The ΛCDM cosmological model – a universe made, primarily, of dynamically cold dark matter (CDM) particles and with accelerated expansion from the cosmological constant (Λ) – makes predictions for the clustering of dark matter through perturbation theory and N-body simulations. From an observational point of view the existence of dark matter from galaxy rotation curves is indisputable and from galaxy-redshift surveys and other measurements we have a very good idea of how the dark matter clusters on cosmological scales.

On galactic scales the clustering of dark matter is harder to assess observationally. Strong gravitational lensing and the observed features in tidal streams around the Milky Way seem to indicate the presence of substructure, predicted by N-body simulations, but more tests need to be done before it is an open and shut case for the existence of small scale dark matter clustering.

References

Abadi, M. G., Bower, R. G., & Navarro, J. F. 2000, MNRAS, 314, 759

Aharonian, F., et al. 2008, Astroparticle Physics, 29, 55

Alcock, C., et al. 1995, Physical Review Letters, 74, 2867

Bertschinger, E. 1998, ARA&A, 36, 599

Bullock, J. S., & Johnston, K. V. 2005, ApJ, 635, 931

Congdon, A. B., & Keeton, C. R. 2005, MNRAS, 364, 1459

Corbelli, E., & Salucci, P. 2000, MNRAS, 311, 441

Dodelson, S. 2003, Modern Cosmology. Amsterdam (Netherlands): Academic Press.

Dalal, N., & Kochanek, C. S. 2002, ApJ, 572, 25

Diemand, J., Kuhlen, M., & Madau, P. 2007, ApJ, 667, 859

Efstathiou, G., Frenk, C. S., White, S. D. M., & Davis, M. 1988, MNRAS, 235, 715

Evans, N. W., & Witt, H. J. 2003, MNRAS, 345, 1351

Geller, M. J., & Huchra, J. P. 1989, Science, 246, 897

Ibata, R., Irwin, M., Lewis, G., Ferguson, A. M. N., & Tanvir, N. 2001, Nature, 412, 49

Ibata, R., Irwin, M., Lewis, G. F., & Stolte, A. 2001, ApJ, 547, L133

Inada, N., et al. 2003, Nature, 426, 810

Jenkins, A., Frenk, C. S., White, S. D. M., Colberg, J. M., Cole, S., Evrard, A. E., Couchman, H. M. P., & Yoshida, N. 2001, MNRAS, 321, 372

Johnston, K. V., Spergel, D. N., & Haydn, C. 2002, ApJ, 570, 656

Kamionkowski, M., & Liddle, A. R. 2000, Physical Review Letters, 84, 4525

Kauffmann, G., White, S. D. M., & Guiderdoni, B. 1993, MNRAS, 264, 201

Keeton, C. R., & Moustakas, L. A. 2008, ArXiv e-prints, 805, arXiv:0805.0309

Klypin, A., Kravtsov, A. V., Bullock, J. S., & Primack, J. R. 2001, ApJ, 554, 903

Klypin, A., Kravtsov, A. V., Valenzuela, O., & Prada, F. 1999, ApJ, 522, 82

Klypin, A., Zhao, H., & Somerville, R. S. 2002, ApJ, 573, 597

Kochanek, C. S., & Dalal, N. 2004, ApJ, 610, 69

Komatsu, E., et al. 2008, ArXiv e-prints, 803, arXiv:0803.0547

Koposov, S., et al. 2007, ArXiv e-prints, 706, arXiv:0706.2687

Lima, M., & Hu, W. 2004, Phys. Rev. D, 70, 043504

Mack, G. D., Beacom, J. F., & Bertone, G. 2007, Phys. Rev. D, 76, 043523

Massey, R., et al. 2007, ApJS, 172, 239

Moore, B., Ghigna, S., Governato, F., Lake, G., Quinn, T., Stadel, J., & Tozzi, P. 1999, ApJ, 524, L19

Navarro, J. F., Frenk, C. S., & White, S. D. M. 1997, ApJ, 490, 493

Owen, J. M., Weinberg, D. H., Evrard, A. E., Hernquist, L., & Katz, N. 1998, ApJ, 503, 16

Owen, J. M., Weinberg, D. H., & Villumsen, J. V. 1998, ArXiv Astrophysics e-prints, arXiv:astro-ph/9805097

Peacock, J. A. 1999, Cosmological Physics, Cambridge, UK: Cambridge University Press.

Peebles, P. J. E. The Large Scale Structure of the Universe. Princeton, N.J., Princeton University Press, 1980. 435 p.

Percival, W. J., et al. 2007, ApJ, 657, 51

Press, W. H., & Schechter, P. 1974, ApJ, 187, 425

Seljak, U., & Warren, M. S. 2004, MNRAS, 355, 129

Sheth, R. K., & Tormen, G. 1999, MNRAS, 308, 119

Sirko, E. 2005, ApJ, 634, 728

Sofue, Y., & Rubin, V. 2001, ARA&A, 39, 137

Spergel, D. N., & Steinhardt, P. J. 2000, Physical Review Letters, 84, 3760

Springel, V., et al. 2005, Nature, 435, 629

Strigari, L. E., Bullock, J. S., Kaplinghat, M., Diemand, J., Kuhlen, M., & Madau, P. 2007, ApJ, 669, 676

Strigari, L. E., Koushiappas, S. M., Bullock, J. S., Kaplinghat, M., Simon, J. D., Geha, M., & Willman, B. 2008, ApJ, 678, 614

Tegmark, M., et al. 2004, ApJ, 606, 702

Uchida, S., & Yoshida, T. 2004, MNRAS, 348, 89

Weinberg, D. H., & Gunn, J. E. 1990, MNRAS, 247, 260

Weinberg, D. H., et al. 2007, American Astronomical Society Meeting Abstracts, 211, #132.10

Zentner, A. R., & Bullock, J. S. 2003, ApJ, 598, 49

Zentner, A. R. 2007, International Journal of Modern Physics D, 16, 763

Zwicky, F. 1933, Helvetica Physica Acta, 6, 110